Journal of Nuclear Materials 397 (2010) 19–26

Contents lists available at ScienceDirect

Journal of Nuclear Materials

journal homepage: www.elsevier.com/locate/jnucmat

Development of fuel-model interfaces: Characterization of Pd containing UO_2 thin films

S. Stumpf [a,*], A. Seibert [a], T. Gouder [a], F. Huber [a], T. Wiss [a], J. Römer [b], M.A. Denecke [b]

[a] European Commission, JRC, Institute for Transuranium Elements, P.B. 2340, 76125 Karlsruhe, Germany
[b] Forschungszentrum Karlsruhe, Institut für Nukleare Entsorgung, P.B. 3640, 76021 Karlsruhe, Germany

ARTICLE INFO

Article history:
Received 19 June 2009
Accepted 26 November 2009

ABSTRACT

The presented work aims to reproducibly prepare UO_2–Pd thin film model systems for spent nuclear fuel in order to further investigate surface reactions of these films under relevant redox conditions. The sputter co-deposition of U and Pd in the presence of O_2 results in the homogeneous distribution of Pd in a crystalline UO_2 matrix. Hereby, Pd is found to be oxidized and to form PdO_x. Heating the films after deposition causes the diffusion of film components and induces a change in surface morphology. Independent of the heating temperature initial UO_{2+x} transforms into UO_2. This is different for the noble metal. At high temperatures (550–840 °C) Pd diffuses into the Si-wafer substrate and forms mixed Pd–Si–U alloys. At moderate temperatures (150–200 °C) Pd solely diffuses within the film matrix and forms micrometer sized metallic particles. These particles are further characterized as being an agglomeration of small nanometer sized spheres.

© 2009 Elsevier B.V. All rights reserved.

1. Introduction

The safety assessment of a nuclear waste disposal requires the fundamental understanding of the UO_2 chemistry in aqueous systems since the reactions at the fuel matrix surface can result in the dissolution of the matrix itself and with this can lead to the release of radionuclides into the groundwater. The processes controlling the dissolution of spent nuclear fuel under a range of proposed waste repository conditions have been the focus of several studies ([1–4] and references therein). The solution redox potential is the critical variable due to the redox sensitivity of UO_2 and the formation of soluble UO_2^{2+} caused by oxidation of U(IV) [2,5]. Radiolysis of groundwater will produce both oxidants ($OH^{\cdot}$, H_2O_2, $HO_2^{\cdot}$, O_2) and reductants (H_2, $H^{\cdot}$, e^-) [6–11]. The mechanisms of spent fuel oxidation under varying conditions are described in literature [12–19].

In several experimental studies on spent fuel corrosion using real or simulated spent fuel, the dissolution has been found slower than expected from the concentrations of generated oxidants during water radiolysis [20,21]. Fuel corrosion rates are reported to be decreased by about four orders of magnitude in the presence of hydrogen [22–25]. In the literature two types of mechanisms are proposed as being responsible for such effects [11]. H_2 can consume radiolytically produced oxidants as well as dissolved U(VI) in homogeneous reactions [26,27]. It is discussed by King and Shoesmith [11] that these effects are of minor importance and cannot explain the efficient suppression of fuel corrosion. Another mechanism proposed by several authors ([11] and references therein) is the heterogeneous reaction at the solid–solution interface where hydrogen directly reduces the fuel matrix. At a temperature range expected in a waste repository (<100 °C) hydrogen should be quite inert [1]. Anyhow, the inhibition of fuel dissolution due to the presence of H_2 is observed already at low temperatures. It was concluded in [1] that H_2 is somehow activated, that is, hydrogen decomposes producing $H^{\cdot}$. If waste container failure is delayed for many thousands of years, it is unlikely that the decomposition of H_2 is achievable by the influence of radiation. It is possible that the spent fuel surface itself will be catalytic for the production of $H^{\cdot}$ since the higher oxides of uranium (U_3O_8/UO_3) as well as mixed oxides (USb_3O_{10}) and intermetallics (UNi_5) are known catalysts used in different fields of redox chemistry and synthesis [28–30]. The influence of different uranium oxide surfaces (UO_{2+x}-pellets, simulated high-burnup UO_2-based fuel/SIMFUEL, CANada Deuterium Uranium/CANDU fuel) on the activation of H_2 was investigated by several authors who ascribe the catalytic activation of hydrogen (and hydrogen peroxide) at $T \geqslant 500$ °C to the oxide matrix itself [2,9,22,31–33]. In contrast to these observations several authors claim the metallic precipitates of Mo, Tc, Ru, Rh and Pd (ε-particles) in spent fuel [34] as being responsible for the activation of H_2 (and H_2O_2) at the fuel surface since late 4d-elements and their alloys are known catalysts for redox reactions [35–39] Nilsson et al. and Ekeroth et al. [35,36,40] even exclude any catalytic activity of the UO_2 matrix. They demonstrate that in solution Pd catalyzes the homogeneous reaction between UO_2^{2+} and H_2 as well as H_2 and H_2O_2. The corresponding heterogeneous reaction

* Corresponding author. Tel.: +49 7247 951234.
E-mail address: silvia.stumpf@ec.europa.eu (S. Stumpf).

0022-3115/$ - see front matter © 2009 Elsevier B.V. All rights reserved.
doi:10.1016/j.jnucmat.2009.11.025

of H_2 activation at the surface of a UO_2 pellet doped with Pd was investigated by Trummer et al. who attribute the activation of hydrogen to the presence of Pd [37,38]. The interpretation of the experimental results by Nilsson et al. and Trummer et al. [35–38] is based on indirect parameters such as the determination of H_2O_2 consumption and the change of UO_2^{2+} concentration in solution with varying concentration of Pd in solution and in the oxide matrix respectively. Such approach indicates the catalytic activity of Pd. However, it does not allow drawing a definite mechanistic conclusion on the processes ongoing at the surface.

It becomes obvious that there is a need for a model system which on the one hand allows to selectively investigate the influence of different fuel components (UO_2, Pd) on the catalytic properties of spent fuel with regard to the decomposition of H_2. On the other hand the model system should offer the possibility to directly measure and monitor surface processes. The actual investigations therefore aim to prepare model surfaces which are confined to a UO_2 matrix doped with different amounts of Pd. The preparation of actinide thin films by sputter deposition has been developed by Gouder and Colmenares [41]. The thin film technique allows an easy and controllable way to produce representative samples of the desired elemental composition by the use of small amounts of starting materials, for example elemental uranium or palladium. Another advantage of this approach is the accessibility of thin films to surface analysis tools, which allow the characterization of surface properties as well as the monitoring of surface reactions. Prior to investigations of the surface redox behaviour it has to be clarified if the prepared thin film analogues exhibit comparable properties as spent fuel. That is, the uranium oxide matrix should be of polycrystalline nature and should have a stoichiometry close to UO_2. Moreover, the sputter co-deposition of uranium and palladium should result in the agglomeration of the incorporated noble metal and in the formation of metallic particles.

In the present paper we describe the preparation of thin film model systems which exhibit the cited features. Hereby, structural investigations are performed by application of spectroscopic (XPS) as well as microscopic methods (AFM, SEM, TEM and XRD).

2. Experimental

2.1. Thin film sputter deposition

Thin films of U–O–Pd were prepared in situ by sputter co-deposition from U (99.9% purity) and Pd (99.9% purity) targets with an O_2 partial pressure up to 1×10^{-6} mbar. The pressure of the sputter gas (Ar 99.9999% purity) was 1×10^{-2} mbar. The Ar-plasma was produced by ionizing the Ar with energetic electrons (50–100 eV) emitted from a hot W cathode. The composition of the U–O–Pd films was controlled by the respective target voltages as well as the oxygen partial pressure. The composition of the films was varied between pure UO_2 up to a U:Pd ratio of 30:70. The deposition rates were about 0.5 monolayers per second. The thickness of the films was calculated from weight difference before and after sputter deposition. For high temperature treatment of the films, the film substrate was maintained at the desired temperature for 5 min after deposition in the preparation chamber under UHV. Then the sample was transferred to the analysis position and XPS spectra were taken at room temperature.

For the spectroscopic investigations by X-ray Photoelectron Spectroscopy (XPS), films of ~10 nm thickness were deposited on single crystalline Si-wafers. For the Atomic Force Microscopy (AFM) measurements, films of about 1 μm thickness were deposited on polycrystalline gold discs (10 mm in diameter, 0.25 mm thickness, 99.99% purity). X-ray Diffraction (XRD) measurements were done on films of 1 μm thickness, deposited on single crystalline Si-wafers. Transmission Electron Microscopy (TEM) measurements required the deposition of ~120 monolayers (36 nm thickness) onto Cu-grids coated with carbon (3.05 mm, 1000 square mesh).

2.2. Thin film characterization

The composition of the sputtered films was determined by XPS, analyzing the U 4f, O 1s and Pd 3d area ratios. Moreover, the corresponding binding energies were used to determine the oxidation state of the film components. XPS spectra were recorded with a hemispherical analyser from Omicron (EA 125 U5). The spectra were taken using Mg K_α (1253.6 eV) radiation with an approximate energy resolution of 1 eV. The background pressure in the analysis chamber was 2×10^{-10} mbar.

The crystallinity of the films was investigated by TEM (H700 HST from Hitachi) and XRD (Philips PW3830 X-ray generator fitted with a Philips PW 2213/20 goniometer including a 1.5 kW copper tube).

The surface morphology was determined by SEM measurements, performed on an environmental scanning electron microscope (Philips ESEM XL 30 FEG) equipped with a backscatter electron detector for imaging. As the prepared films were electrically conducting their elemental composition could be analyzed by EDX without a conducting surface coating which may impair backscatter diffraction bands. Moreover, EDX mapping was performed allowing the determination of the distribution of film elements at the surface.

A commercial AFM (Topometrix, TMX 2000, Explorer) was used for the topographic characterization of the thin films. A series of AFM images was recorded in contact-mode using triangular cantilevers with silicon nitride tips (tip radius <50 nm).

3. Results and discussion

3.1. Preparation of UO_2–Pd thin films at room temperature

In order to find the appropriate oxygen partial pressure for the preparation of the UO_2 films, uranium was first sputtered at varying oxygen pressures. The corresponding XPS spectra of the U 4f states are shown in Fig. 1. The spectra exhibit a double line structure with an energy separation of about 11 eV, which are attributed to the spin–orbit split $4f_{5/2}$ and $4f_{7/2}$ lines. The energy positions as well as the shape of the satellite peaks at high binding energy (BE) allow the qualitative speciation of the uranium oxide [42–45]. Evaluation of the U 4f/O 1s area ratios finally allows a quantitative speciation.

According to literature the U $4f_{7/2}$ binding energy (BE) in metallic uranium is 377.4 eV [46]. The films deposited at a O_2 partial pressure of 5×10^{-9} mbar (Fig. 1, lowest curve) can be therefore attributed to the pure metal (measured BE: 377.4 eV). With increasing O_2 pressure the lines decrease in intensity and new features appear on their high BE sides, at 381 eV and 392 eV. These energy positions correspond to UO_2, which is deposited simultaneously with elemental uranium. At an O_2 pressure of 1×10^{-7} mbar the lines at 377.4 eV and 388.3 eV disappear showing that all of the deposited uranium is oxidized. The energy separation between satellite and main line, which is 7 eV, is characteristic for UO_2. Formation of this oxide is confirmed by the U 4f/O 1s intensity (area) ratios. With further increase of the oxygen pressure, the satellite broadens taking a shape typical for the higher uranium oxide UO_{2+x} [42] which is quantified as being $UO_{2.3}$.

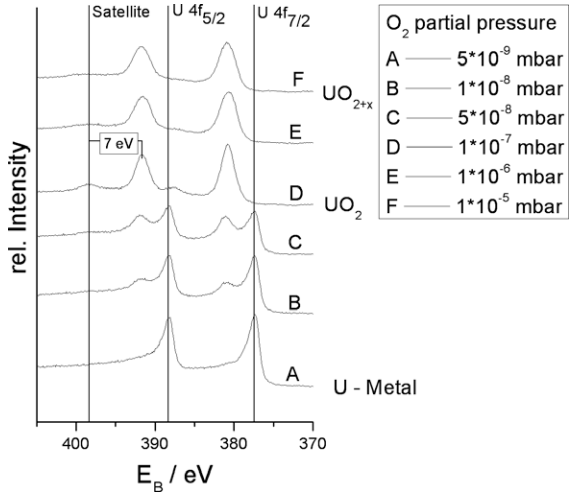

Fig. 1. U 4f spectra of U sputtered at different O_2 partial pressures. UO_2 is generated at 1×10^{-7} mbar O_2.

In a next step, the uranium oxide was loaded with Pd, by co-depositing U and Pd in presence of oxygen (1×10^{-7} mbar). Formation of UO_2 was confirmed by the corresponding U 4f spectra (not shown here). The noble metal concentration was varied by varying the U and Pd deposition rates, via adjustment of the respective target voltages/currents. The spin orbit split Pd 3d lines of the experimental series are shown in Fig. 2.

At a Pd concentration of 60%, the two lines at BEs of 335.4 eV ($3d_{5/2}$) and 340.7 eV ($3d_{3/2}$) are attributed to the deposition of pure Pd metal [46]. The weak satellite at 346.7 eV is related to the unfilled d-band ($4d^{9.3}$) of the noble metal [47,48]. With decreasing palladium concentration the Pd signal intensity decreases. Furthermore, the satellite disappears (zoom in Fig. 2). This points to the filling of the Pd 4d band with decreasing Pd concentration. Such filling is equal to the loss of band structure and with this to the loss of metallic character. The Pd 3d lines slightly broaden indicating the generation of chemically modified Pd atoms. At a concentration of 16% Pd, the Pd line develops an intense feature at 2.5 eV higher BE that can be attributed to the formation of a new Pd species. Although Pd is a known noble metal its oxidation is reported in literature. The chemical shift of the Pd 3d peak of PdO is quoted between +1.3 eV and +1.9 eV [47,49] and for PdO_2 between +2.1 eV and +2.9 eV [49]. Even the formation of PdO_3 has been proposed by some authors (shift ~+3.5 eV) [50,51]. Based on these investigations we propose the observed peaks at 337.9 eV and 343.2 eV as being due to the oxidation of Pd and most likely the formation of PdO_2. With further lowering the Pd concentration, the Pd metal signals disappears in favour of the PdO_2 band. Surprisingly, the deposition of Pd alone in the presence of oxygen does not result in the oxidation of the noble metal even at $p(O_2) = 1 \times 10^{-6}$ mbar (own measurements; spectra not shown here).

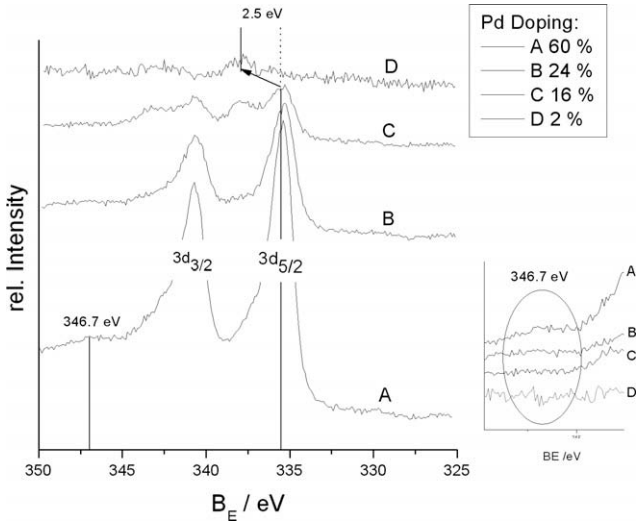

Fig. 2. Pd 3d spectra for the UO_2–Pd co-deposition with decreasing Pd concentration.

The XRD diffractograms of thin films with varying Pd concentration are given in Fig. 3a. The selected diffraction peaks can be attributed to crystalline UO_2 (cubic fluorite structure) [52]. With increasing Pd concentration (from 3% to 17% Pd) the peaks undergo a slight shift of $\Delta 2\theta = \sim +0.3$ as compared to the given UO_2 reference spectrum. The observed shift corresponds to a smaller lattice parameter and with this indicates a distortion of the oxide matrix. At a Pd concentration of 30% the reflexes even disappear which points to the amorphisation of the matrix. Reflexes characteristic of a metallic Pd phase (ε-particles) are not detected. The TEM image of a film with 14% Pd doping is given in Fig. 3b. The TEM diffraction pattern together with the monitored Bragg circles

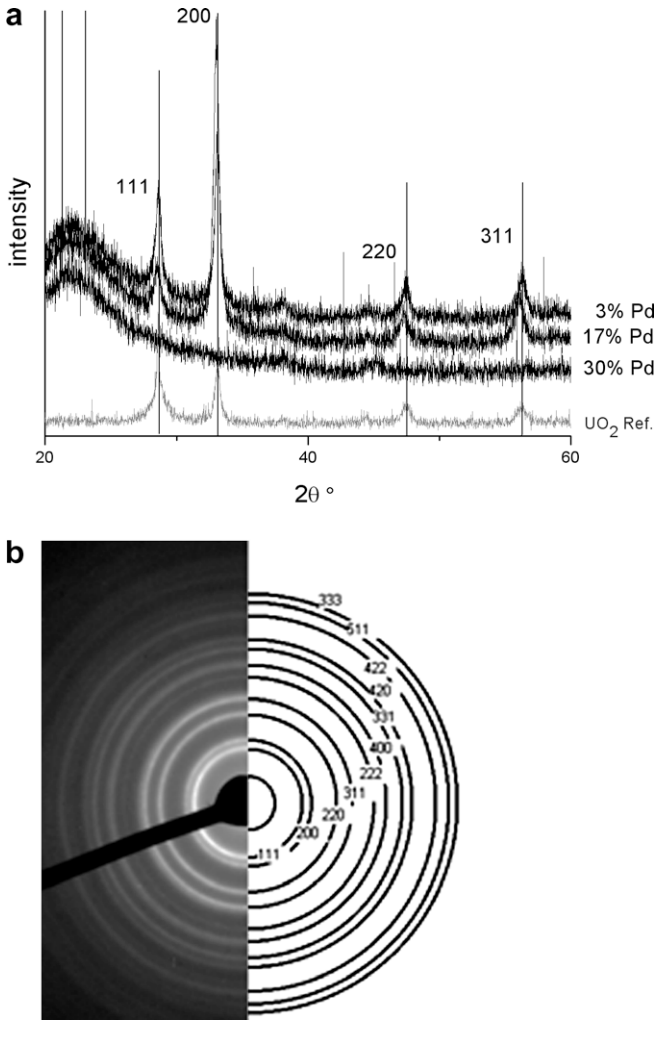

Fig. 3. (a) XRD diffractogram of UO_2–Pd thin films at varying Pd concentration. For comparison a UO_2 reference diffractogram is also given. The UO_2 matrix exhibits crystallinity (cubic fluorite structure). With increasing Pd concentration the diffraction peaks are shifted by $\Delta 2\theta = \sim +0.3$, decrease and rather vanish. (b) Bragg cycles of a thin film with 14% Pd inclusion measured with TEM. The pattern can be attributed to crystalline UO_2 (cubic fluorite structure).

indicates the presence of polycrystalline UO_2. Reflexes corresponding to a metallic Pd phase are not detected which is in good accordance with the above described XRD results.

In order to obtain more insight into the composition of the sputtered films we also applied EDX analysis. The EDX mapping of a UO_2–Pd thin film (40% Pd; 250 μm * 200 μm detail) (Fig. 4) clearly shows that uranium (light gray) and palladium (dark gray) both are evenly distributed over the entire area. Local enrichment or depletion of one element in favour of the other is not observed. Taking the XRD results into account, the homogeneous distribution of film components is equivalent to the dissolution of Pd in UO_2. Such interpretation could explain the observed distortion and even amorphisation (at 30% Pd content) of the crystalline oxide matrix. Several authors report on the decrease of the UO_2 fluorite unit cell size due to dissolved fission product atoms in irradiated and simulated spent fuels [34,53–56]. Lucuta et al., who investigated the microstructural features of SIMFUEL by XRD, ascribe the lack of Pd diffraction peaks to the small concentration of the noble metal in the UO_2 matrix [57]. In the present study, we additionally propose the lack of Pd peaks as being due to the lack of a metallic Pd phase and the formation of an oxide surface with mixed stoichiometry where Pd is partly oxidized ($Pd/PdO_x/UO_y$) as it was shown by XPS. We assume that the sputter deposition procedure is responsible for such phenomenon. Since the substrate is hold at room temperature during sputtering the plasma is abruptly cooled at the surface. That is, the arrangement of components in the plasma is frozen in the deposited film and the fast cooling down does not allow further movement of the components on the surface. With this, the film more or less represents a snapshot of a system state which is not necessarily thermodynamically stable. During the sputter process enough oxygen is supplied and, in contrast to palladium, uranium is easily oxidized. The homogeneous distribution of Pd in UO_2 results in its dilution and in the separation of Pd atoms. This makes an agglomeration to metallic particles difficult. By contrast, the only binding partner which is accessible to Pd is represented by excessive oxygen. The noble metal is finally oxidized.

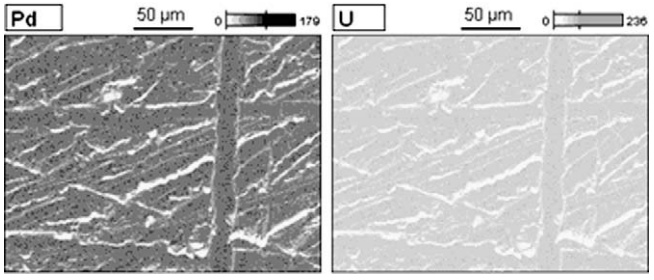

Fig. 4. EDX mapping image of a UO_2–Pd film (40% Pd) sputtered at room temperature. Pd and U are homogeneously distributed over the surface.

3.2. Preparation of UO_2–Pd thin films at higher temperatures

At temperatures between 400 °C and 1700 °C ε-particles form in nuclear fuel [10]. To prepare similar ε-particles in thin films, several samples were heated after deposition on the Si-wafer. As an example, the XPS overview spectra of a UO_{2+x} film doped with 70% Pd and heated from room temperature (RT) to successively higher temperatures, up to 840 °C, are shown in Fig. 5a.

The continuous increase of the U/Pd ratio with increasing temperature is striking and points to the diffusion of thin film components already at temperatures of 550 °C. The evolution of the U 4f, O 1s and Pd 3d area ratios indicate that U diffuses to the surface replacing Pd. The oxygen concentration at the surface stays unchanged. During diffusion U transforms from initial UO_{2+x} into UO_2, which is confirmed by the shape of the corresponding U 4f detail spectra (not shown here) and the calculation of the U/O ratio. The initial Pd 3d spectrum can be attributed to the metal, which seems to be plausible at this high nobel metal concentration of 70%. However, with increasing temperature the peak intensity decreases and the shape of the Pd 3d lines changes. At 650 °C a shoulder at 336.9 eV appears in the spectrum which replaces the main line with a further increase in temperature. The intensity decrease of the Pd 3d lines indicates that the surface is depleted in Pd, probably due to Pd diffusion out of the UO_2–Pd film into the underlying Si-substrate. The Pd 3d line at 1.7 eV higher BE can be either attributed to Pd alloying with U [58,59] or Pd oxidation (see discussion above). The Pd 3d spectra in Fig. 5b do not allow discriminating between these two options. The formation of Pd–U alloys seems unlikely since this requires the breaking of U–O bonds which are very stable and the reduction of the oxide to metallic uranium which is not observed in the spectrum. By contrast, alloying with Si could be an explanation. Si is detectable in the XPS spectrum beginning with

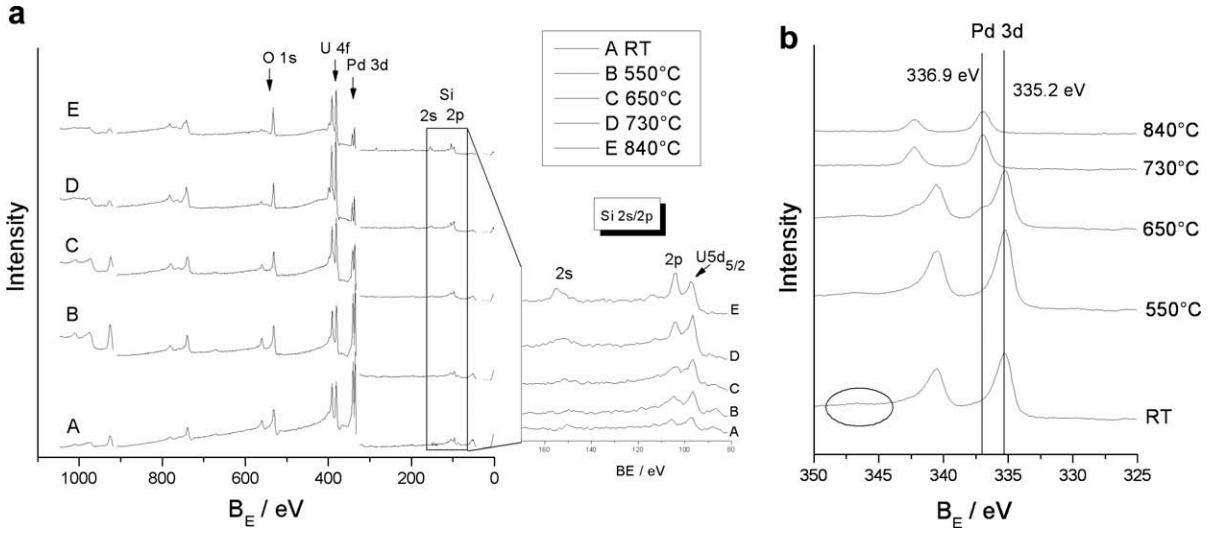

Fig. 5. (a) XPS overview spectra of a thin film composed of UO_{2+x} doped with 70% Pd. Heating the film up to 840 °C after deposition results in a change of the U/Pd ratio and Si appears in the spectrum. (b) The corresponding Pd 3d spectra are shifted to higher BEs during heating. The satellite at 346.7 eV disappears.

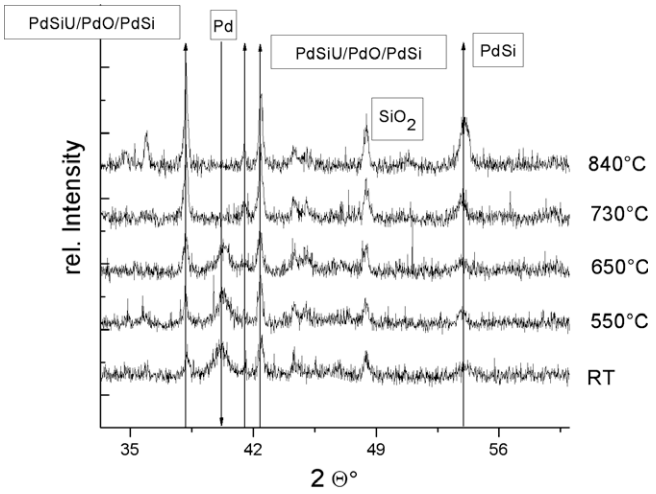

Fig. 6. XRD diffractograms of a UO_2–Pd (70%) thin film deposited on a Si-substrate and heated in several steps from room temperature up to 840 °C. The Pd peak disappears whereas new peaks appear that indicate alloying processes.

a temperature of 650 °C (Fig. 5a; zoom). Additional XRD measurements confirm that the Pd depletion of the surface is associated with Pd–Si alloying. The Pd peak in the XRD diffractogram at $2\theta = 40.3°$ decreases and finally disappears with increasing temperature whereas new peaks appear in the spectrum that can be attributed to PdSi, PdSiU and PdO [60] (Fig. 6).

As consequence of this finding, the sputtered films were then repeatedly heated to moderate temperatures after deposition. The XPS spectra of a UO_{2+x}–Pd (Pd = 16%) film annealed in several cycles for maximum 2 min at temperatures between 150 °C and 200 °C are shown in Fig. 7. The spectra are referenced to the O 1s peak position of the room temperature sample.

As observed above at a Pd concentration of about 16%, the initial Pd 3d spectrum after room temperature deposition exhibits two features at ~336 eV and ~338 eV for the Pd $3d_{3/2}$ line, which are attributed to Pd metal and Pd oxide, respectively. With increasing number of heating cycles, the features in the Pd 3d spectrum that can be attributed to Pd oxide decrease and finally disappear. Due to heating the broad peak shape becomes narrow. Hereby, the right side of the peak stays unchanged whereas only the contribution at high BEs disappears. The peak intensity slightly increases during

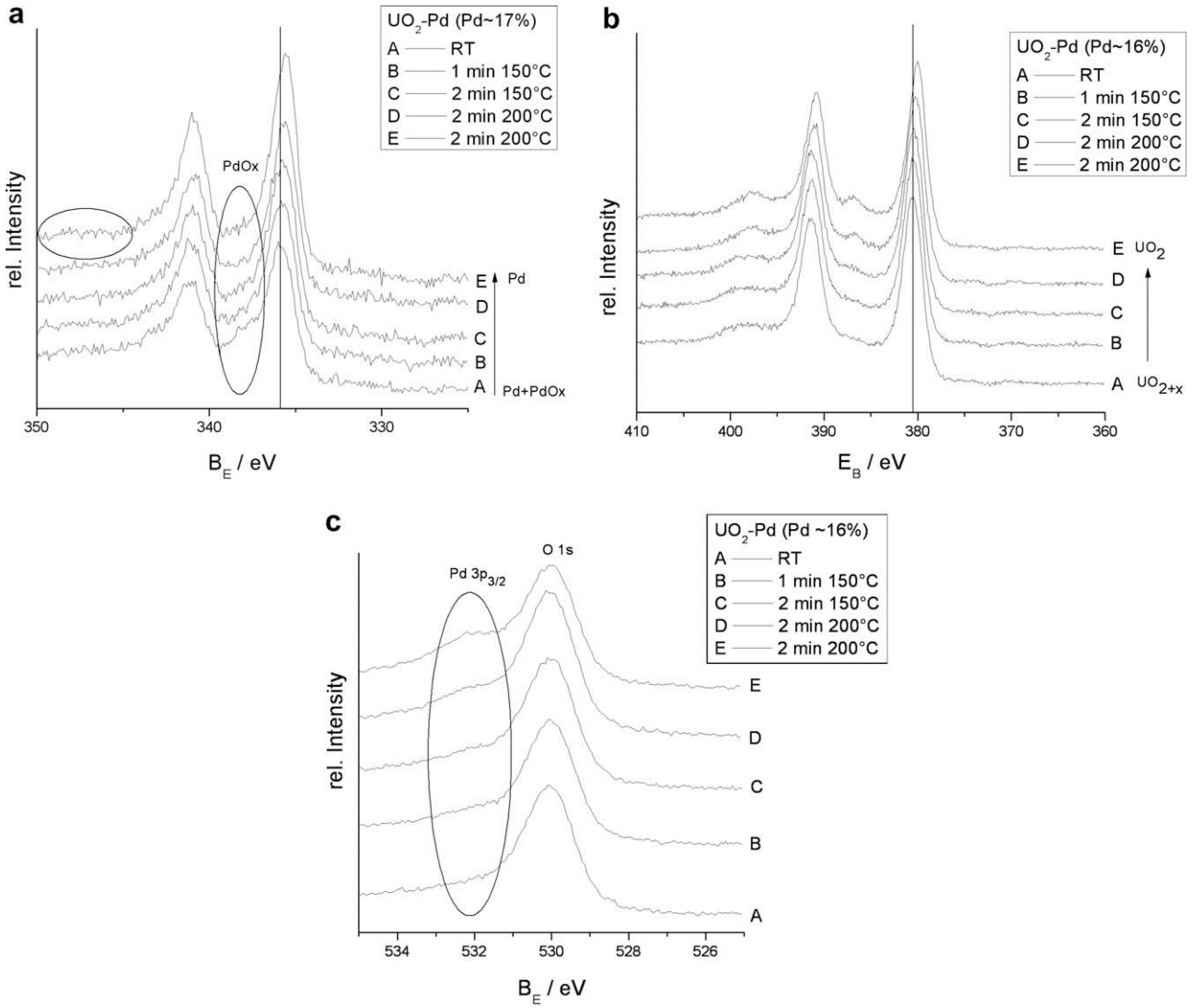

Fig. 7. XPS spectra of a thin film composed of UO_{2+x} doped with 16% Pd and heated several times to moderate temperature. (a) Pd 3d: due to heating the PdO_x feature disappears; the broad spectra undergo a narrowing; the peak intensity increases; a satellite at 346.7 eV is evolving. (b) U 4f: due to heating U transforms from UO_{2+x} to UO_2; the broad spectra undergo a narrowing; the intensity increases. (c) O 1s: due to heating the Pd 3p feature increases.

heating and a satellite at 347 eV BE develops. The final spectrum of the series is slightly shifted to lower BEs by 0.3 eV. U is deposited as hyperstoichiometric UO_{2+x}, as shown by the satellite in the initial U 4f spectrum (Fig. 7b). The temperature treatment results in the narrowing of the U 4f bands together with a slight increase of signal intensity. Moreover, the satellites at 386.4 eV and 397.5 eV are more pronounced. Again, the final spectrum of the series is slightly shifted to lower BEs by 0.3 eV. In the O 1s detail spectra an additional peak at ~532 eV develops during heating which can be attributed to Pd $3p_{3/2}$. In contrast to the observed increase in intensity for Pd 3d and U 4f, the O 1s signal slightly decreases.

The change in the Pd 3d, Pd 3p and U 4f spectral features indicates the diffusion of film components already at such moderate temperatures. The disappearance of the "PdO_x" signal in the Pd 3d lines together with the generation of the satellite can be attributed to the reduction of the oxide to the metal. The initial broad shape gives evidence that the room temperature sputtered films exhibit defect structures with atoms in high energy positions which in photoemission appear at high BEs. These structures disappear during heating due to healing, thus leading to line narrowing. The slight increase in peak intensity confirms such interpretation, since the smoothing of the surface results in an increase of the photoemission yield. This also accounts for the development of the corresponding U 4f spectra. Again, the narrowing of the peaks together with an increase in intensity and a pronounced satellite structure stands for a diffusion process and a smoothing of the film surface, where UO_{2+x} is reduced to UO_2. Obviously, the reduction of PdO_x and UO_{2+x} involves the diffusion of excessive oxygen down into the matrix which could explain the O 1s intensity decrease. The free surface space is finally filled with Pd and U which could additionally explain the enrichment of both components at the surface (higher intensity + visibility of the less sensitive Pd 3p feature). The observed shift of about 0.3 eV for the final spectra of the series cannot be explained at this point.

The interpretation of XPS data is well confirmed by XRD measurements of the heated samples shown in Fig. 8. In contrast to the room temperature deposited films the diffraction peaks are not significantly shifted as compared to the given UO_2 reference. Even at higher Pd concentrations of about 28%, diffraction peaks that can be attributed to crystalline UO_2 still are visible. These results give evidence that heating involves a recrystallization process which comprises the development of a less distorted UO_2 lattice. This may imply that Pd segregates even though no Pd peaks are detectable in the XRD diffractogram.

Additionally, it is possible monitoring the change of film morphology due to heating by AFM. The AFM images of a UO_2–Pd film (Pd = 16%) sputtered at room temperature and heated afterwards for 2 min at 200 °C are comparatively shown in Fig. 9a.

The surface of a film sputtered and analyzed at room temperature shows the homogeneous coverage by ~100 nm sized crystallites. Heating the films leads to the formation of larger crystallites of about 350 nm in size. This confirms our previous assumption that the film components diffuse, leading to a structural reorganization/recrystallization of the film surface. In addition, heating the Pd doped films leads to the appearance of spherical particles with a diameter of 1–3 μm, on top of the surface (Fig. 9b). The particles stick about 70 nm out of the surface. The SEM image of such a particle is shown in Fig. 10. The particle consists of an agglomeration of much smaller spheres (0.3–1 μm), which are not resolved by AFM. The EDX analysis confirms that these agglomerates consist of Pd and thus support the assumption that a segregation process

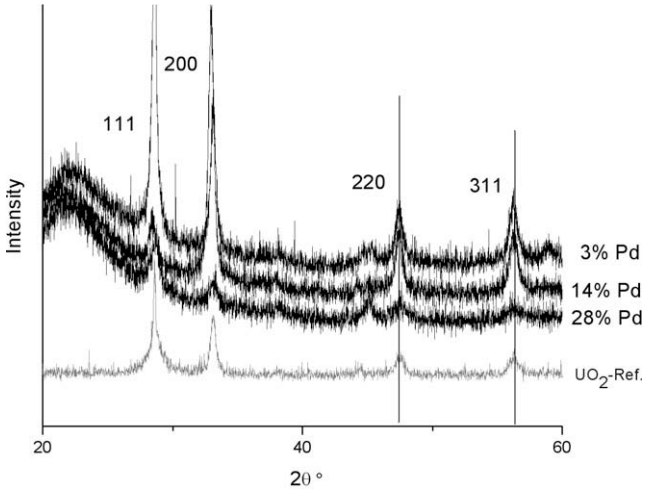

Fig. 8. XRD diffractogram of UO_2–Pd thin films at varying Pd concentration heated after deposition at 200 °C for 3 × 2 min. For comparison a UO_2 reference spectrum is also given. The reflexes are not shifted as compared to the given UO_2 reference.

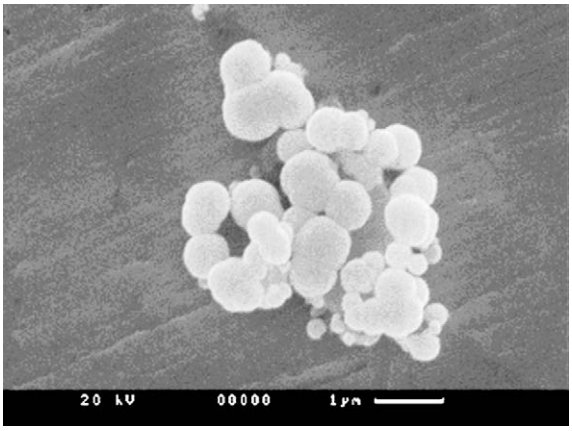

Fig. 10. SEM image of the UO_2–Pd film (Pd = 16%) sputtered at room temperature and heated afterwards at 200 °C for 2 min. The particles on top of the film surface are characterized as being an agglomeration of 0.3–1 μm sized Pd spheres (ε-particles).

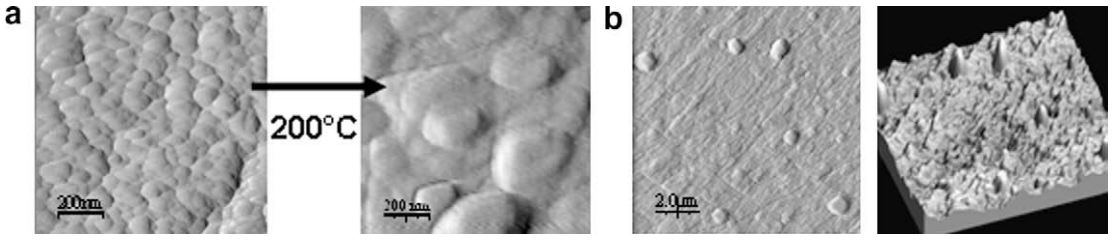

Fig. 9. AFM images of a UO_2–Pd film (Pd = 16%) sputtered at room temperature and heated afterwards at 200 °C for 2 min. (a) The 100 nm sized film crystallites become larger (350 nm) due to the heating procedure. (b) Spherical particles (1–1.5 μm) are formed on top of the surface.

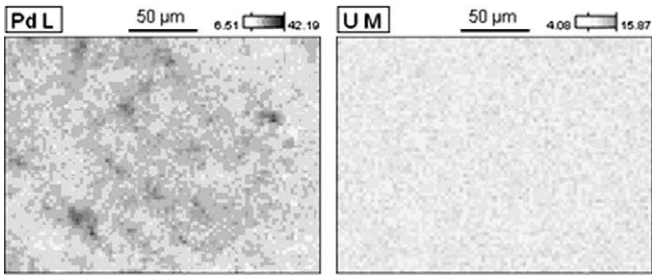

Fig. 11. EDX mapping image of the UO_2–Pd film (Pd = 16%) sputtered at room temperature and heated afterwards at 200 °C for 2 min. The Pd ε-particles are randomly distributed over the surface.

at the surface finally results in the formation of ε-particle analogues. The characterized agglomerates are well comparable with mixed alloy particles (ε-particles) extracted from spent fuel by Cui et al. [39]. This again supports our approach of preparing spent fuel model surfaces.

The EDX mapping image of the film heated at 200 °C is shown in Fig. 11. In contrast to the mapping image of the non-annealed film (Fig. 4) we observe a local enrichment of Pd, while uranium stays homogeneously distributed over the surface. The Pd agglomerates are not evenly distributed which indicates the formation of ε-particles at preferential sites of the surface.

4. Conclusion

Thin film model systems for spent nuclear fuel are successfully prepared by sputter co-deposition of U and Pd in the presence of O_2. The surface composition as well as the chemical state of the system is monitored by photoemission spectroscopy (XPS). Variation of the U and Pd target currents and the O_2 pressure provide a control of the concentration of the Pd-inclusion as well as the oxidation state of U.

As a first result the characterization of the thin film surfaces sputtered at room temperature clearly shows that the sputter technique allows the generation of a UO_{2+x} matrix which is very close to a spent fuel matrix regarding the uranium oxidation state of IV (generation of UO_2 at 1×10^{-7} mbar O_2 partial pressure) and the matrix crystallinity (cubic fluorite structure) respectively. However, the EDX spectra indicate that, due to the U–Pd co-deposition, Pd is homogeneously distributed in the UO_2 matrix and distorts the oxides crystal lattice (XRD measurements). Moreover, XPS spectra indicate the oxidation of the noble metal during co-deposition at room temperature and the authors propose the formation of a mixed oxide film (Pd–PdO_x–UO_{2+x}).

Heating the mixed UO_2–Pd films results in the diffusion of film components and involves in change of film morphology. Initial UO_{2+x} is reduced to stoichiometric UO_2. In contrast to the films sputtered at room temperature, the XRD diffractograms of the high temperature films correspond to the ones of pure UO_2 and no lattice distortion is detectable. By high temperature treatment (550–840 °C) Pd diffuses into the Si-wafer matrix and forms Pd–Si as well as Pd–U alloys. At moderate temperatures (maximum 200 °C) the diffusion of film components results in the enrichment of Pd at the surface and causes the generation of Pd agglomerates. The Pd agglomerates resemble quite well ε-particles found in spent nuclear fuel.

The investigations show that the thin film technique is well suitable for the preparation of model systems for spent nuclear fuel since the sputtered films comply with the stated requirements such as crystallinity of the uranium oxide matrix and the formation of ε-particles. Based on the described preparative results, first investigations of the electrochemistry of fuel-model interfaces are now being performed.

References

[1] L.H. Johnson, D.W. Shoesmith, Spent fuel, in: W. Lutze, R.C. Ewing (Eds.), Radioactive Waste Forms for the Future. North-Holland, Amsterdam, 1988, pp. 635–698.
[2] D.W. Shoesmith, J. Nucl. Mater. 282 (2000) 1–31.
[3] E.C. Buck, B.D. Hanson, B.K. McNamara, The geochemical behaviour of Tc, Np and Pu in spent nuclear fuel in an oxidizing environment, in: Energy Waste and the Environment: A Geochemical Perspective, The Geological Society of London Special Publication 236, 2004, pp. 65–88.
[4] L. Johnson, C. Ferry, C. Poinssot, P. Lovera, J. Nucl. Mater. 346 (2005) 56–65.
[5] D.W. Shoesmith, S. Sunder, W.H. Hocking, in: J. Lipkowski, P.N. Ross (Eds.), Electrochemistry of Novel Materials, VCH, New York, 1994, pp. 297–337.
[6] S. Sunder, Atomic Energy of Canada Limited Report, AECL-11380, COG-95-340, 1995.
[7] F. King, M. Kolar, Ontario Power Generation Report No. 00819-REP-01200-10041-ROO, 1999.
[8] J.W.T. Spinks, R.J. Woods, in: An Introduction to Radiation Chemistry, John Wiley and Sons Inc., New York, 1964, pp. 477–480.
[9] M.E. Broczkowski, J.J. Noel, D.W. Shoesmith, J. Nucl. Mater. 346 (2005) 16–23.
[10] J. Bruno, R.C. Ewing, Elements 2 (2006) 343–349.
[11] F. King, D.W. Shoesmith, SKB Technical Report TR-04-20, 2004, pp. 1–26.
[12] O. Roth, M. Jonsson, Cent. Eur. J. Chem. 6 (2008) 1–14.
[13] S. Sunder, D.W. Shoesmith, N.H. Miller, J. Nucl. Mater. 244 (1997) 66–74.
[14] V.V. Rondinella, H. Matzke, J. Cobos, T. Wiss, Radiochim. Acta 88 (2000) 527–531.
[15] D.W. Shoesmith, L.H. Johnson, Ontario Hydro Report No. 06819-REP-01200-0012 R00, 1997.
[16] J.C. Wren, D.W. Shoesmith, S. Sunder, J. Electrochem. Soc. 152 (2005) 470–481.
[17] H. Christensen, S. Sunder, Nucl. Technol. 131 (2000) 102–123.
[18] D.W. Shoesmith, M. Kolar, F. King, Corrosion 59 (2003) 802–816.
[19] C. Poinssot, C. Ferry, P. Lovera, C. Jegou, J.M. Gras, J. Nucl. Mater. 346 (2005) 66–77.
[20] M. Jonsson, F. Nielsen, O. Roth, E. Ekeroth, S. Nilsson, M.M. Hossain, Environ. Sci. Technol. 41 (2007) 7087–7093.
[21] T.E. Eriksen, M. Jonsson, SKB Technical Report TR-07-06, 2007, pp. 1–19.
[22] K. Spahiu, L. Werme, U.B. Eklund, Radiochim. Acta 88 (2000) 507–511.
[23] S. Röllin, K. Spahiu, U.B. Eklund, J. Nucl. Mater. 297 (2001) 231–243.
[24] K. Spahiu, J. Devoy, D. Cui, M. Lundström, Radiochim. Acta 92 (2004) 597–601.
[25] K. Spahiu, D. Cui, M. Lundström, Radiochim. Acta 92 (2004) 625–629.
[26] M. Jonsson, F. Nielsen, E. Ekeroth, T.E. Eriksen, in: V.M. Oversby, L.O. Werme (Eds.), Mater. Res. Soc. Symp. Proc., vol. 807, Materials Research Society, Warrendale, PA, 2004, pp. 385–390.
[27] T. Lundstrom, in: Proc. Spent Fuel Workshop 2002, 23–25 September, 2002, Avignon, France.
[28] C.A. Colmenares, Prog. Solid State Chem. 15 (1984) 257–364.
[29] P. Diaz-Arocas, J. Quinones, C. Maffiotte, J. Serano, J. Garcia, J.R. Almazan, J. Esteban, Mater. Res. Soc. Symp. Proc. 353 (1995) 641–646.
[30] H. Christensen, R. Forsyth, L. Lundquist, L.O. Werme, Studsvik Report NS-90/85, Studsvik Energiteknik AB, Nyokoping, Sweden, 1992.
[31] S. Sunder, N.H. Miller, D.W. Shoesmith, Corros. Sci. 46 (2004) 1095–1111.
[32] H.W.G. Heynen, C.G.M. Camp van Berkel, H.S. van der Baan, J. Catal. 48 (1977) 386–394.
[33] B. Bunji, B. Zogovic, in: Proceedings of the International Symposium on Peaceful Uses of Atomic Energy, Stockholm, 1958, pp. 350–355.
[34] H. Kleykamp, J. Nucl. Mater. 131 (1985) 221–246.
[35] S. Nilsson, M. Jonsson, J. Nucl. Mater. 372 (2008) 160–163.
[36] S. Nilsson, M. Jonsson, J. Nucl. Mater. 374 (2008) 290–292.
[37] M. Trummer, S. Nilsson, M. Jonsson, J. Nucl. Mater. 378 (2008) 55–59.
[38] M. Trummer, O. Roth, M. Jonsson, J. Nucl. Mater. 383 (2009) 226–230.
[39] D. Cui, J. Low, C.J. Sjöstedt, K. Spahiu, Radiochim. Acta 92 (2004) 551–555.
[40] E. Ekeroth, M. Jonsson, T.E. Eriksen, K. Ljungqvist, S. Kovacs, I. Puigdomenech, J. Nucl. Mater. 334 (2004) 35–39.
[41] T.H. Gouder, C.A. Colmenares, Lawrence Livermore National Laboratory, UCRL-ID-118664, 1994, pp. 1–38.
[42] Y.A. Teterin, V.M. Kulakov, A.S. Baev, N.B. Nevzorov, I.V. Melnikov, V.A. Strelsov, L.G. Mashirov, D.N. Suglobov, A.G. Zelenkov, Phys. Chem. Minerals 7 (1981) 151.
[43] S. van den Berghe, J.P. Laval, B. Gaudreau, H. Terryn, M. Verwerft, Nucl. Mater. 277 (2000) 28–36.
[44] S. Bera, S. Sali, S. Sampath, S.V. Narasimhan, V. Venugopal, J. Nucl. Mater. 255 (1998) 26–33.
[45] B.G. Santos, H.W. Nesbitt, J.J. Noel, D.W. Shoesmith, Electrochim. Acta 49 (2004) 1863–1873.
[46] J.F. Moulder, W.F. Stickle, P.E. Sobol, K.D. Bomben, in: Handbook of X-Ray Photoelectron Spectroscopy, Perkin Elmer Corporation, Physical Electronic Division, USA, 1992.
[47] K.S. Kim, A.F. Gossmann, N. Winograd, Anal. Chem. 46 (1974) 197–200.
[48] F.U. Hillebrecht, J.C. Fuggle, P.A. Bennett, Z. Zolnierek, Phys. Rev. B 27 (1983) 2179–2193.
[49] J.M. Tura, P. Regull, L. Victori, Surf. Interface Anal. 11 (1988) 447–449.
[50] A.E. Bolzan, A.C. Chialvo, A.J. Arvia, J. Electroanal. Chem. 179 (1984) 71–82.

[51] J. Genesca, L. Victori, Rev. Coat. Corros. 4 (1981) 325–348.
[52] P.E. Tomaszewski, Phase Transit. 38 (1992) 127–220.
[53] J.H. Davies, F.T. Ewart, J. Nucl. Mater. 41 (1971) 143–155.
[54] J.M. Leitnaker, J. Nucl. Mater. 51 (1974) 95–105.
[55] T. Adachi, T. Muromura, H. Takeishi, T. Yamamoto, J. Nucl. Mater. 160 (1988) 81–87.
[56] M. Ugajin, K. Shiba, J. Nucl. Mater. 105 (1982) 211–218.
[57] P.G. Lucuta, R.A. Verrall, J. Nucl. Mater. 178 (1991) 48–60.
[58] R. Eloirdi, T. Gouder, F. Wastin, J. Rebizant, J. Alloys Compd. 372 (2004) 10–16.
[59] A. Bzowski, T.K. Sham, Phys. Rev. B 48 (1993) 7836–7840.
[60] I. Engstroem, Acta Chem. Scand. 24 (1970) 1466–1468.